Astronomical and Astrophysical Transactions (*AApTr*), 2019, Vol. 31, Issue 2, pp. 89–102,
ISSN 1055-6796, Photocopying permitted by license only, ©Cambridge Scientific Publishers

Features of evolution of the magnetic field gradient in solar active region before a strong flare

A.A. Solov'ev[1,2,*], V.E. Abramov-Maximov[1], V.N. Borovik[1], L.V. Opeikina[3], A.G. Tlatov[1,2]

[1] *Central Astronomical Observatory at Pulkovo (Russian Academy of Sciences), Saint-Petersburg, Russia*
[2] *Kalmyk State University, Elista, Russia*
[3] *Special Astrophysical Observatory (Russian Academy of Sciences), Nizhnii Arhiz, Russia*

Received 1 October, 2018

The research of solar active regions (ARs) on pre-flare phase (during a few days before the flare) can reveal features in microwave emission of AR and its magnetic-field characteristics that indicate that a powerful flare is about to take place. The aim of this research is to study the evolution of radio and magnetographic characteristics of two ARs (NOAA 11520 and 12242), where a strong flare occurred. We analyzed microwave emission and magnetic-field characteristics of ARs as based on RATAN-600 and SDO data. In this study we focused on the behavior of magnetic field gradient and distance between regions of maximum magnetic fields of opposite polarities. We find that initially the distance between regions of maximum magnetic fields of opposite polarities is decreased. Then it begins to increase. On the phase of its increasing the flare occurred. An MHD model of magnetic flux rope describes well the observed events.

Keywords: Sun: flares, Sun: magnetic fields, magnetohydrodynamics (MHD)

1 Introduction

The first evidence of the relationship of flare activity with the magnetic field structure of the active region (AR) were obtained more than 50 years ago. Künzel (1960) came to the conclusion that the formation of the δ-configuration is the most significant precursor of high flare activity of the AR. Severnyi (1960) revealed a close relationship between the occurrence of flares and peculiarities of structure of the magnetic field. Recently some authors (Schrijver, 2016; Harra et al., 2016; Toriumi et al., 2017) concluded that the most characteristic sign of the preparation of a large flare is the formation of a magnetic field structure of the "SHIL" (Strong-field, High-gradient polarity Inversion Line) type.

*Email: solov.a.a@mail.ru

The first evidence of the existence of microwave sources, projected on the neutral line of photospheric magnetic field, and their connection with flares have been obtained from the solar eclipse observations on March 7, 1970 (Quinones et al., 1975). Observations of the Sun on Westerbork Synthesis Radio Telescope (WSRT) at a wavelength of 6 cm revealed quasi-stationary bright sources above the neutral line in flare-active ARs (Kundu et al., 1977; Kundu and Alissandrakis, 1984).

Regular multiwavelength spectral-polarization solar radio observations at the RATAN-600 radio telescope, begun in 1975, revealed "peculiar" radio sources in the ARs. They were appearing before large flares and were situated above the areas of the maximum gradient of photospheric magnetic field near the neutral line (Akhmedov et al., 1986).

Daily observations using the Nobeyama Radioheliograph (NoRH) at a wavelength of 1.76 cm have shown that the sources above the neutral line of the magnetic field (neutral line associated source – NLS) are typical and often dominant sources in ARs, in which large flares occur. A relationship was found between the appearance of NLS and the beginning of a flare (Uralov et al., 2008). The appearance and development of these sources is connected with the occurrence of large flares and can be considered as a prognostic factor.

New results were obtained in recent years due to the new observation capabilities, in particular, magnetographic observations on the space observatory SDO and observations in microwave band on a radio telescope RATAN-600 with the use of a new multi-octave spectral-polarization high-resolution complex (Bogod et al., 2011).

Observations of several ARs in 2011–2015 on RATAN-600 showed that for 1–2 days before the flare of X-class (according to classification of GOES) in the microwave emission of the AR was registering a new (in most cases, dominant) microwave source (NLS), which was associated with the place of the maximum magnetic field gradient above the neutral line of photospheric magnetic field (Abramov-Maximov et al., 2015a). The evolution of this source is similar to the evolution of the magnetic field gradient (Abramov-Maximov et al., 2015b). Simultaneous magnetographic analysis showed a rapid increase in the horizontal gradient of the magnetic field. The X-flare occurred 5–20 hours after the total gradient of the magnetic field of the entire AR reached its maximum value (Abramov-Maximov et al., 2017).

The aim of this work is to continue the cycle of authors' work to study ARs on pre-flare phase. In this paper, we focus on analyzing the dynamics of the magnetic field gradient and the distance between the regions of the maximum magnetic fields of opposite polarities, as well as on the theoretical explanation of the mechanism of the flare, based on presented observational facts.

2 Observations

We have considered two ARs in which flares of X-class occurred: NOAA 11520 (X1.4, 12.07.2012, 16:49UT) and NOAA 12242 (X1.8, 20.12.2014, 00:28UT).

We used data obtained on RATAN-600 radio telescope and space observatory Solar Dynamics Observatory/Helioseismic and Magnetic Imager (SDO/HMI) (Scherrer et al., 2012). RATAN-600 observations were carried out with multi-octave Spectral and polarization high-resolution system (SPHRS) (Bogod et al., 2011) at local noon

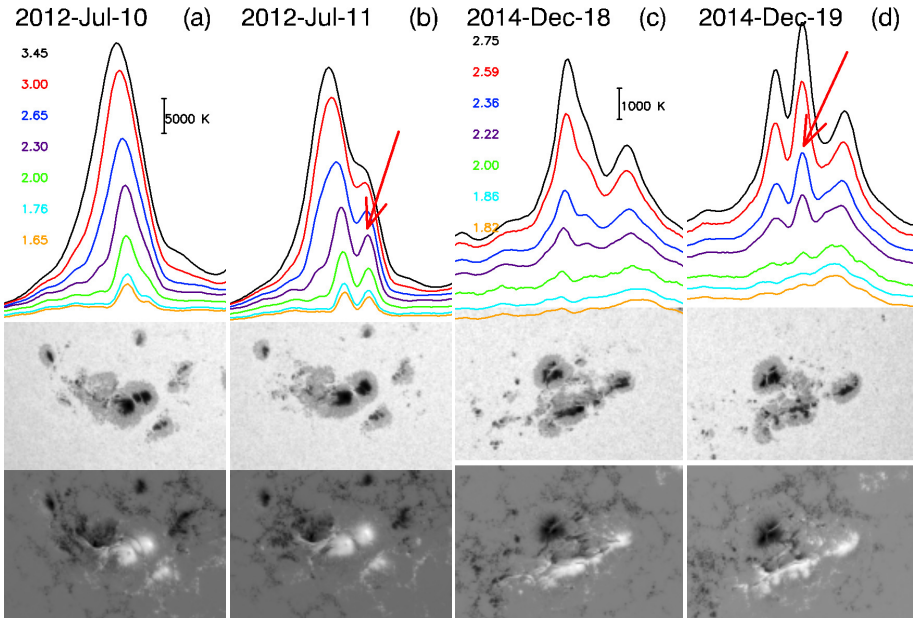


Figure 1 Fragments of one-dimensional solar scans in the microwave range in the intensity channel (Stokes parameter I) obtained with the RATAN-600. Panels (a) and (b) – NOAA 11520, (c) and (d) - NOAA 12242. Wavelengths (centimeters) and vertical scale (antenna temperatures) are given in panels (a) for NOAA 11520 and (c) for NOAA 12242. Images in the continuum and magnetograms according to SDO/HMI data are given under the scans. The red arrows indicate the neutral-line associated sources.

and in some azimuths with different positions angles of the Sun. Observations in azimuths allow us to fulfill two-dimensional identification of radio sources with continuum images and magnetograms. See details of observations and data processing in (Abramov-Maximov et al., 2015a). Magnetographic parameters are calculated using the method proposed by Tlatov et al. (2014).

Fragments of radio scans are showed in Fig. 1. In both cases the following features are revealed. About 2 days before the flare, we observe the appearance of the microwave source, located above the neutral line of the photospheric magnetic field. It is shown by red arrow. The identification of a new microwave source, made using the observations at RATAN-600 in different azimuths with different positional angles of the Sun, showed that the new source is uniquely identified with the region near the neutral line.

Simultaneously with the increase of the intensity of the source, the total gradient of the magnetic field increases and the distance between the regions of the maximum magnetic fields of opposite polarities located near the neutral line decreases. After reaching its maximum value, the gradient of the magnetic field begins to decrease, and the distance between the regions of the maximum magnetic fields of opposite polarities, respectively, increases. The flare occurs at this stage.

Figure 2a shows a total magnetic field gradient (in arbitrary units) of NOAA

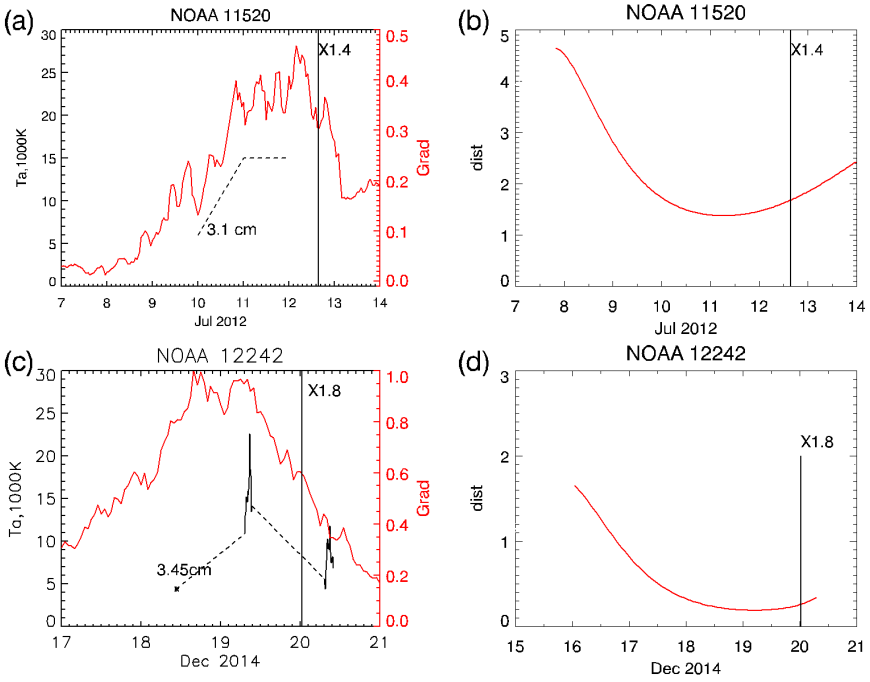


Figure 2 (a) The total magnetic field gradient (red solid curve, right axis, in arbitrary units) of NOAA 11520 and the intensity of the microwave source above the neutral line at a wavelength of 3.1 cm (black dashed curve, left axis, antenna temperatures) as observed by RATAN-600. The moment of flare X1.4 is marked by a vertical line. (b) The distance (in arbitrary units) between the regions of maximum magnetic fields of opposite polarities for AR 11520. (c) The total magnetic field gradient (red solid curve, right axis, in arbitrary units) of the NOAA 12242 and the intensity of the microwave source above the neutral line at a wavelength of 3.45 cm (black dashed curve, left axis, antenna temperatures) as observed by RATAN-600. (d) The distance (in arbitrary units) between the regions of maximum magnetic fields of opposite polarities for 12242.

11520. The moment of flare X1.4 is marked by a vertical line. Figure 2c shows the total gradient of the magnetic field NOAA 12242 and the intensity of the microwave source above the neutral line at a wavelength of 3.45 cm as observed by RATAN-600. Figures 2b and 2d show the distance between the regions of maximum magnetic fields of opposite polarities for ARs 11520 and 12242, respectively.

3 Model

3.1 Concept

Based on described features of the development of the flare in configurations with approaching magnetic centers, it is possible to propose the following scenario for the development of a flare process in such events.

The first stage is the approach of magnetic centers (spots) of different polarity. In this case, the spots, like two moving bulldozers strongly compress the magnetic flux between the spots. This ensures the accumulation of magnetic energy, which will subsequently be released in the flare.

At the second stage a current magnetic structure is formed (magnetic flux rope) between the sunspots above the neutral line of the magnetic field as a result of the process of magnetic reconnections. This structure has a sufficiently strong non-potential magnetic field and has a large supply of free (associated with electric currents) magnetic energy. A clear indication of this process is the appearance of a bright inter-sunspot microwave source in the region between the spots, which is formed due to the appearance of energetic charged particles accelerated in numerous small-scale current sheets that arise during the formation of a magnetic flux rope. At the moment of maximum closeness of the spots, the filament is kept from eruption by the external magnetic field connected two sunspots of opposite polarity. Physical conditions in the magnetic filament are already close to the threshold for the occurrence of plasma instabilities in it, but this threshold has not yet been reached.

At the third stage, the process of separation of sunspots begins. The external field, which plays a critical role in ensuring the equilibrium of the configuration, is weakening. This causes a change in the equilibrium in the magnetic flux rope, in a twisted magnetic power tube, in which strong electric currents flow according to equilibrium conditions. At this stage, a region with very low plasma density develops in the magnetic flux rope. The current velocity of the electrons becomes compared with the thermal velocity of the ions, and this serves as a trigger for the excitation of plasma instabilities (Bernstein modes, ion sound ...). These instabilities give rise to an avalanche of plasmons effectively dissipating the ordered fluxes of electrons carrying the electric charge. This very quickly and sharply (by many orders of magnitude) reduces the conductivity of the plasma in the flux rope. Abnormal resistance heats the plasma. The strong electric field that occurs when the current channel is "locked" causes the particles acceleration and appearance of the runaway electrons, that in fact leads to the development of the flare process (Solov'ev, Murawski, 2014; Solov'ev, Kirichek, 2015).

It should be noted that the formation of the flare configuration occurs quite slowly. Its characteristic time, about a day, considerably exceeds the relaxation time of the system to equilibrium, which is not more than a few minutes. Therefore, the process of preparation of the flare can be described as a quasi-static process, in which the system successively passes through a continuous sequence of equilibrium states.

Our goal in this case is to propose a magnetohydrostatic model. This model should describe the equilibrium of a nonpotential magnetic filament compressed by an external transverse field, which has a large supply of free magnetic energy and an extremely inhomogeneous plasma density distribution in its cross-section. It is important that this inhomogeneous plasma distribution must be parametrically sensitive with respect to small variations of the external magnetic field strength and the height of the magnetic flux rope over the photosphere. Then we can get the main effect of the model. With a decrease in the external field compressing the flux rope and/or a slight increase in the height of the center of the flux rope over the photosphere (these two effects simulate the process of divergence of spots), the inhomogeneity in the distribution of the plasma density increases. The resulting plasma density, which

consists of the background hydrostatic value and the additive to it, due to the magnetic force, takes in critically small values in some part of the magnetic flux rope (in fact, it tends to zero according to the equilibrium conditions). When the degree of rarefaction of charge carriers in a magnetic flux rope with current passes the threshold of excitation of plasma instabilities, flare energy release is switched on during a fraction of a second.

3.2 Magnetohydrostatic simulation

Let us assume that the magnetic flux rope formed between the approaching spots is sufficiently long. It also corresponds to the conditions of translational symmetry, when none of its parameters changes noticeably along the filament axis. Consider a straight filament, located horizontally in a plane stratified atmosphere. The filament is invariant with respect to arbitrary displacements along one of the coordinates (directed along its axis). Suppose that in the Cartesian coordinates x, y, z this is the y axis, so $\partial/\partial y = 0$. The z-axis is directed vertically upwards, counting from the surface of the photosphere. Gravity is expressed as $F_g = -\rho g(z) e_z$. The system of equations of magnetic hydrostatics that ensure the equilibrium of such magnetic configuration is:

$$-\nabla P + (4\pi)^{-1}[curl\mathbf{B} \times \mathbf{B}] - \rho g(z) e_z = 0 \tag{1}$$

$$div\mathbf{B} = 0 \tag{2}$$

$$P = \rho \Re T \mu^{-1} \tag{3}$$

Here: $\mathbf{B}$ – magnetic field strength, P – pressure, ρ – density, T – temperature of the gas, μ – average molar mass. In the case of translational symmetry, the system (1)–(3) reduces to the form (Low, 1975):

$$\Delta A = -\frac{1}{2}\frac{dB_y^2(A)}{A} - 4\pi\frac{dP(A,z)}{dA} \tag{4}$$

$$\rho(A,z)g(z) = -\frac{\partial P(A,z)}{\partial z} \tag{5}$$

$$T(x,z) = \frac{\mu}{\Re}\frac{P(x,z)}{\rho(x,z)} \tag{6}$$

Here: $\Delta = \dfrac{\partial^2}{\partial x^2} + \dfrac{\partial^2}{\partial z^2}$ – Laplace operator, $A(x,z) = \int_0^x B_z dx$ – flux of vertical magnetic field through a rectangular horizontal pad of unit width (in the direction of the axis y) and length z. The equation $A(x,z) = const$ determines the geometric form of the magnetic field lines in the projection onto the plane x, z.

The poloidal field components in accordance with equation (2) are expressed by the derivatives:

$$B_z = \frac{\partial A}{\partial x}, B_x = -\frac{\partial A}{\partial z} \tag{7}$$

The longitudinal field $B_y(A)$ due to the translational symmetry of the system depends only on the magnetic flux $A(x,z)$.

Let us define the magnetic structure of the filament, i.e. we assume that the functions $A(x,z)$ and $B_y(A)$ are known. We shall find, by integrating the equation

(4), the equilibrium pressure distribution corresponding to these magnetic profiles. Then from equation (5) we calculate the density distribution in the system. And further from equation (6) we calculate the temperature profile of the filament. Thus, for any given magnetic configuration we can find the thermodynamic parameters which correspond to its equilibrium state (Solov'ev, Murawski 2014).

Let us suppose that the flux function has the form:

$$A(x,z) = B_0 \frac{z - z_0}{1 + l^2(z - z_0)^2 + k^2 x^2} - b_x \cdot (z - z_0), \tag{8}$$

where B_0 – a constant specifying the scale of the magnetic field strength, k, l – the transverse and vertical scales of the filament, respectively, z_0 – a constant that regulates the position of the filament in height relative to the photosphere (level $z = 0$), b_x – a positive constant that determines the strength of external magnetic field. This magnetic field holds the filament from the eruption (the second term in (8)) (see Fig. 3). Note that $b_x \ll B_0$. The distribution (8) is symmetric in x with respect to the origin. Therefore, the magnetic filament described by it will be located, in accordance with our concept, between the sunspots above the photospheric neutral line of inversion of the magnetic polarities.

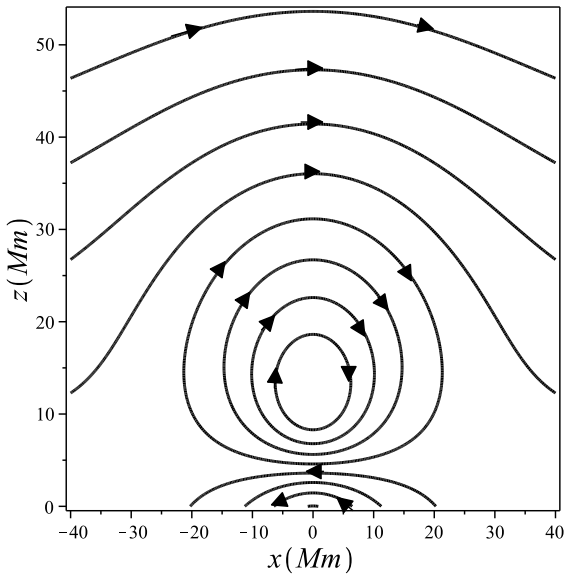


Figure 3 The cross-section of a long magnetic filament held from above by an external magnetic field. The shape of the magnetic field lines is obtained from condition $A = const$. Assumed: $z_0 = 4Mm$, $k = 0.1Mm^{-1}$, $b_x = 0.1B_0$. The longitudinal magnetic field $B_y(A)$ in the figure is not displayed.

To simplify the model for $B_y(A)$ in equation (4) we adopt the hypothesis of a homogeneous longitudinal field: $B_y^2(A) = b_y^2 \equiv const$. Thus, the background magnetic field where the magnetic flux rope is located will be equal to $\mathbf{B}_{ex} = b_x \mathbf{e}_x + b_y \mathbf{e}_y \equiv const$.

After substituting this expression and the function (8) into the Laplace operator, equation (4) takes on the form:

$$\frac{B_0(z-z_0)(6l^2+2k^2)}{4\pi(1+l^2(z-z_0)^2+k^2x^2)^2}-\frac{8B_0(z-z_0)(l^4(z-z_0)^2+k^4x^2)}{4\pi(1+l^2(z-z_0)^2+k^2x^2)^3}=\frac{dP(A,z)}{dA}.$$

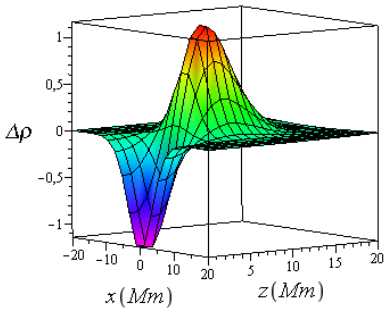


Figure 4 Addition to the background density of the hydrostatic atmosphere caused by the magnetic field of the filament (in units $B_0^2k(\pi g)^{-1}$). Parameters: $z_0 = 4Mm$, $k = 0.1Mm^{-1}$, $b_x = 0.2B_0$. The lengths are given in Mm. At the level $z = z_0$, the plasma density in the filament is equal to the density of the external medium, below – a rarefied cavity is formed, above – the area is denser than the corona.

If we assume that the vertical and transverse scales of the filament are equal, i.e. $l = k$, then the left-hand side of the equation is greatly simplified:

$$\frac{8B_0k^2(z-z_0)}{4\pi(1+k^2(z-z_0)^2+k^2x^2)^3}=\frac{dP(A,z)}{dA}$$

or:

$$\frac{2k^2[A+b_x(z-z_0)]^3}{\pi B_0^2(z-z_0)^2}=\frac{dP(A,z)}{dA}. \tag{9}$$

Equation (9) is very easily integrated with respect to the variable A for a fixed z:

$$\frac{k^2[A^4+4A^3b_x(z-z_0)+6A^2b_x^2(z-z_0)^2+4b_x^3A(z-z_0)^3]}{2\pi B_0^2(z-z_0)^2}+P_{ex}(z)=P(A,z) \tag{10}$$

As the integration constant, the pressure of the external medium $P_{ex}(z)$ is used. We find the density distribution from equations (5) and (10), differentiating (10) with respect to the variable z for fixed A:

$$\rho(A,z)=\rho_{ex}(z)+\frac{k^2}{\pi gB_0^2}\Big[\frac{A^4}{(z-z_0)^3}+\frac{2A^3b_x}{(z-z_0)^2}-2Ab_x^3\Big] \tag{11}$$

In equations (10) and (11), $P_{ex}(z)$ and $\rho_{ex}(z)$ mean the pressure and density of the external medium, which are given by the modern model of the solar atmosphere

(Avrett, Loeser, 2008) and can be considered known. Finally, returning to the variables (x, z), we obtain explicit expressions for calculating the equilibrium distributions of pressure and density in the filament:

$$P(x,z) = P_{ex}(z) + \frac{B_0^2}{8\pi} 4k^2 (z - z_0)^2 [F^4 + \frac{b_x}{B_0} F^3 + (\frac{b_x}{B_0})^2 F^2 + (\frac{b_x}{B_0})^3 F], \quad (12)$$

$$\rho(x,z) = \rho_{ex}(z) + \frac{B_0^2}{8\pi g} 8k^2 (z - z_0)[F^4 + 2\frac{b_x}{B_0} F^3 - 2(\frac{b_x}{B_0})^3 F]. \quad (13)$$

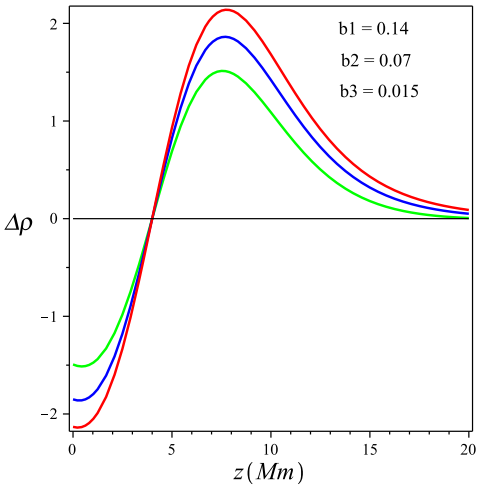


Figure 5 Increase of the amplitude of the magnetic additive to the density (the second term on the right-hand side of (13)) with a decrease in the strength of the external magnetic field on the central axis ($x = 0$). The decrease b_x arising from the discrepancy of the spots leads to an increase in the negative value of the additive to the density at the origin. The additive profile is given in units of $\frac{B_0^2 k}{\pi g}$.

Here is denoted

$$F(x,z) \equiv \frac{A}{B_0(z - z_0)} = \frac{1}{1 + k^2(z - z_0)^2 + k^2 x^2} - \frac{b_x}{B_0}. \quad (14)$$

All lengths are measured in Mm, and the inverse scales are measured in 1/(Mm). The plasma density in this model rapidly decreases with distance from the axis, both in the vertical and in the transverse direction. At the level $z = z_0$, the gas density in the filament is equal to the density of the external medium. Above this level, the additive to the background density is positive, and lower is negative, that is, starting from this level, a dense part of the filament is formed in the corona above the transition zone, and in its chromosphere is its sparse part, due to which a flare process in this area becomes possible. Figure 4 shows the surface shape describing the form of the "magnetic additive" (the second term on the right side of (13)) to the plasma

density in the filament. Figure 5 shows an ncrease in the amplitude of the magnetic additive to the density with a decrease in the strength of the external magnetic field. Figure 6 shows the shift of the altitude profile of the magnetic additive to the density (on the x = 0 axis) with an increase in the height of the center of the flux rope above the level of the photosphere.

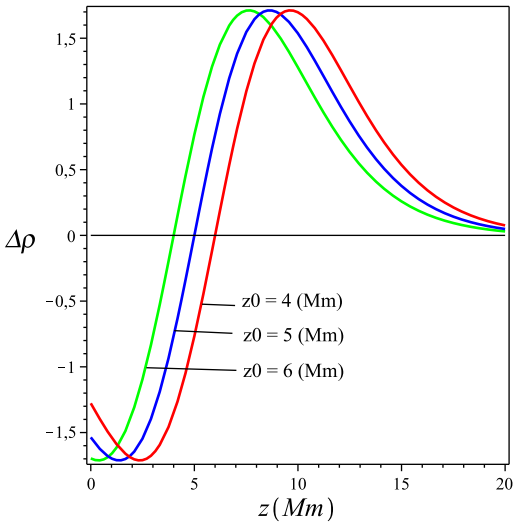


Figure 6 Shift of the altitude profile of the magnetic additive to the density (on the x = 0 axis) with an increase in the height of the center of the flux rope above the level of the photosphere. When the filament is raised, the profile shifts to the right, without changing the amplitude, but at a height of 2.5 Mm (red line) the background plasma density $\rho_{ex}(z)$ in equation (13) falls seven orders of magnitude (!) compared to the photospheric one. So, the resultant density in the lower part of the flux rope with such an upward shift can quickly go through zero. Negative density has no meaning, it simply means that there is no equilibrium solution in this case.

Let us consider two numerical examples. Figure 7 shows the dependence of density on height obtained from equation (13) for some typical values of the parameters. It can be seen that in some regions the density of the plasma becomes arbitrarily small, as the magnetic flux rope is raised into rarefied layers of the solar atmosphere. The parameter b_x here remained fixed.

The effect of decreasing the external field b_x is shown in Fig. 8.

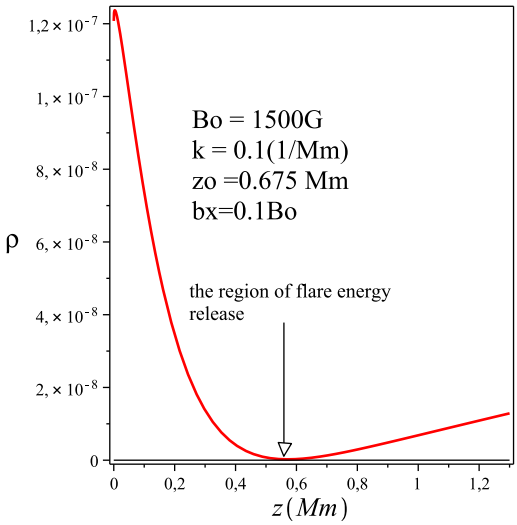


Figure 7 Density distribution with parameters: $B_0 = 1500G$, $k = 0.1Mm^{-1}$, $z_0 = 0.63Mm$.

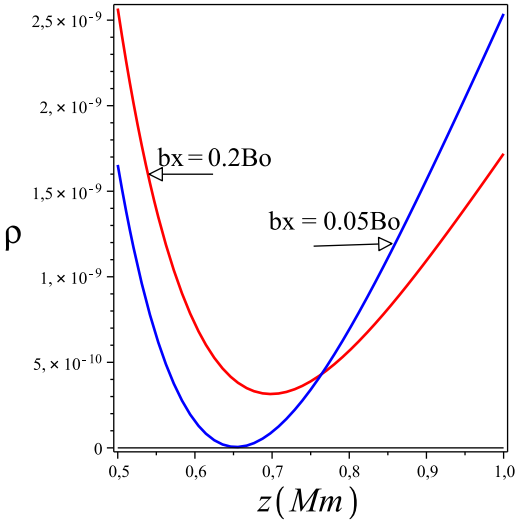


Figure 8 Two distributions of the density in the flux rope for different values of the transverse external field. A decrease in this field (the blue curve) leads to an effective decrease in the density in some region. That is the trigger of the flare.

4 Conclusion

We study the evolution of microwave radiation and the magnetographic characteristics of AR 11520 and 12242, where X-class flares occurred. In both cases development of a new microwave source was recorded before the flare. It was found that the new source was identified with the place of greatest convergence of fields of opposite polarity near the neutral line of the photospheric magnetic field. We find that the total magnetic field gradient firstly increased, and then, after passing through the maximum, it decreased immediately before the X-flare. The distance between the centers of regions of opposite polarity first decreased, and then, having reached its minimum, began to increase.

A similar conclusion was made by Korsos et al. (2015). Using SOHO/MDI-Debrecen Data they found that before large flares there is a sharp increase in the gradient of the magnetic field, followed by its decrease before the flare.

A MHD model of magnetic flux rope which describes well the observed events is proposed. According to this model, as the sunspots converge, energy accumulation takes place. Then, with the discrepancy of the sunspots, flare energy release begins.

Acknowledgements

We acknowledge support from the Presidium of Russian Academy of Sciences, Program KP19-270. A.S. and A.T. were supported by the Russian Scientific Foundation (project 15-12-20001). We are grateful to the SDO team for the SDO/HMI data. We thank the staff of the Special astrophysical observatory of the Russian Academy of Sciences for observations of the Sun with the RATAN-600.

References

Abramov-Maximov V.E., Borovik V.N., Opeikina L.V., Tlatov A.G. (2015a) Solar Phys., 290, 53

Abramov-Maximov V.E., Borovik V.N., Opeikina L.V., Tlatov A.G. (2015b) Geomagnetism and Aeronomy, 55, 1097.

Abramov-Maximov V.E., Borovik V.N., Opeikina L.V. et al. (2017) Geomagnetism and Aeronomy, 57, 978

Akhmedov Sh.B., Borovik V.N., Gelfreikh G.B. et al. (1986) Astrophys. J., 301, 460

Avrett, E.H., Loeser R. (2008) Astrophys. J. Suppl. Ser., 175, 229

Bogod V.M., Alesin A.M., Pervakov A. (2011) Astrophysical Bulletin, 66, 223

Harra L.K., Schrijver C.J., Janvier M. et al. (2016) Solar Phys., 291, 1761

Korsos M.B., Gyenge N., Baranyi T., Ludmany A. (2015) Journal of Astrophysics and Astronomy. 36, Issue 1, 111

Kundu M.R., Alissandrakis C.E., Bregman J.D., Hin A.C. (1977) Astrophys. J., 213, 278

Kundu M.R., Alissandrakis C.E. (1984) Solar Phys., 94, 249

Künzel H. (1960) Astron. Nachr., 285, 271

Low B.C. (1975) Astrophys. J., 197, 251
Quinones J.A., Korzhavin A.N., Peterova N.G., Santos J. (1975) Soln. Dannye, 3, 87 (in Russian)
Severnyi A.B. (1960) Izvestia Krimskoi astrofiz. obs., 22, 12 (in Russian)
Schrijver C.J. (2016) Astrophys. J., 820, Id. 103
Scherrer P.H., Schou J., Bush R.I., Kosovichev A.G. et al. (2012) Solar Phys., 275, 207
Solov'ev A.A., Murawski K. (2014) Astrophysics and Space Science, 350, No.1, 11
Solov'ev A.A., Kirichek E.A. (2015) Astronomy Letters, 41, no.5, 211
Tlatov A.G., Vasil'eva V.V., Makarova V.V., Otkidychev P.A. (2014) Solar Phys., 289, 1403
Toriumi S., Schrijver C.J., Harra L.K. et al. (2017) Astrophys. J., 834, Id. 56
Uralov A.M., Grechnev V.V., Rudenko G.V. et al. (2008) Solar Phys., 249, 315